Laser Processing of Titanium Aluminides

Sherman McElroy, Dehua Yang, and Ramana G. Reddy

(Submitted 23 October 1999; in revised form 1 June 2000)

Using a Nd-YAG laser, laser processing of a series of Ti-Al alloys including pure Ti and Ti-Al intermetallic compounds has been studied. Scanning electron microscopy (SEM), x-ray photoelectron spectroscopy (XPS), and optical microscopy were used to determine the surface morphological, chemical, and compositional characteristics of the laser-processed samples. Analysis of results showed that cracks along grain boundaries caused by rapid heating and cooling of laser processing were the dominant characteristics of the surface morphologies of the laser-processed samples. The Al content in the Ti-Al alloys played a very important role in crack initiation and/or development. The more Al content in the samples, the more severe the cracks that developed after laser processing under the same conditions. The experiments were conducted at ambient conditions, resulting in surface oxidation layers being observed on the processed samples. The XPS results indicated that the oxidation layer consisted of adsorbed O_2, Al_2O_3, TiO_2, and TiO. In addition, Al enrichment was found in the oxide film of TiAl as well as in the oxidation layers formed on the surfaces of TiAl and Ti_3Al intermetallics that were processed by the laser; this differs from the reported results for traditional oxidation of TiAl at elevated temperature.

Keywords intermetallics, laser processing, microscopy, titanium alloys

1. Introduction

In the last few years, there has been an enormous increase in research and development activity on titanium aluminides, in particular, on the Ti-Al compounds, since theyhave immense potential as new high-temperature lightweight structural materials.[1] Based on their many attractive properties such as high melting point, low density, high modulus, high density strength ratio, high strength at elevated temperatures, and good oxidation resistance, titanium aluminide alloys have been identified as candidates for aerospace materials for future generations of both jet engines and airframes.[2] As a structural alloy, machinability and fabricability represent important considerations in determining potential alloy application.[3] However, literature search results indicate that, on one hand, tremendous efforts have been given to the study of the microstructure/property relationships, improvement of room-temperature ductility, and mechanical properties of titanium aluminides.[4–7] On the other hand, machining and fabrication aspects of these intermetallics have not received the attention they deserve.

Laser processing of materials has been developing for more than 20 years since the 1970s when laser technology started to boom. To date, it has been widely accepted by industry in applications such as cutting, welding, drilling, and surface modification in the aim of improving surface-related properties of materials. The advantages of laser-processed material over other material processing technology are highly localized and low-in-total heat input, which minimizes the distortion of the work piece; high density and concentrated energetic beam, as the only needed tool that produces very high local heating and cooling rates of materials; higher production rates; greater flexibility; and automatic controllability in industrial applications. Laser welding has been used on many kinds of materials including ferrous alloys, aluminum and its alloys, and titanium and its alloys.[8] Not only has laser cutting been applied to various materials,[9,10,11] but many mathematical and computational models for laser cutting have also been developed recently.[12,13] Nevertheless, few papers[3,14] on the laser processing of titanium aluminides have been found.

Therefore, to explore the possibility of applying laser processing on titanium aluminides and to help in understanding of laser processing of titanium aluminides in the future, primary laser melting experiments have been conducted on $TiAl_3$, TiAl, and Ti_3Al intermetallics as well as pure Ti and Al alloys using a Nd-YAG laser. The surface morphological and compositional characteristics were examined using scanning electron microscopy (SEM), optical microscopy, and x-ray photoelectron spectroscopy (XPS). The experimental results and discussion are presented below.

2. Experimental

The titanium aluminide samples used for laser processing are Ti_3Al, TiAl, and $TiAl_3$. They were made by means of arc melting of raw materials, *e.g.*, 99.9 wt.% pure Ti wires and 99.9 wt.% pure Al rods, in a copper hearth under flow of purified argon using tungsten electrodes. The arc melting procedure was repeated to ensure homogeneity.[4,5,6] The titanium aluminide ingots were later homogenized at 1273 K for 18 h in argon atmosphere.[15,16] Then, the samples were cut using a diamond saw from the ingot rods into pieces with the required thickness. In addition to the titanium aluminide samples, pure cast Ti and commercial 2024 Al alloy samples were also used in the laser processing experiments. All the samples were polished using 600 grit SiC papers, cleaned ultrasonically in acetone, and dried

Sherman McElroy, Dehua Yang, and **Ramana G. Reddy**, Department of Metallurgical and Materials Engineering, The University of Alabama, Tuscaloosa, AL 35487. Contact e-mail: rreddy@coe.eng.ua.edu.

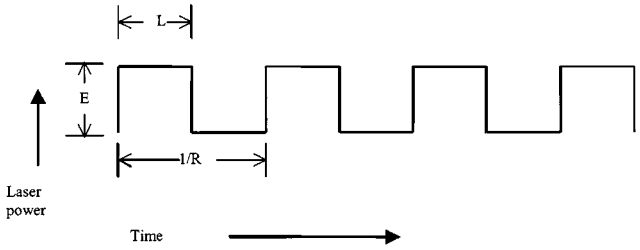

Fig. 1 Schematic illustration of laser pulse shape and control parameters

Table 1 The main compositions and sizes of sample used for laser processing

Samples	Ti (at.%)	Al (at.%)	Size (mm)(a)
Ti	99.9	. . .	10 d × 3.2 t
Ti_3Al	68	32	10 d × 3.2 t
TiAl	51	49	10 d × 3.2 t
$TiAl_3$	28	72	10 d × 1.6 t
2024	Trace	>92	12 × 12 × 3.2 t

(a) d, diameter; and t, thickness

with compressed air before laser processing. The compositions and sizes of the samples are given in Table 1.

An Electrox (Hertfordshire, UK) Scorpion 400W Nd:YAG laser was used to process the surfaces of the samples at various processing parameters. As illustrated in Fig. 1, three laser parameters can be easily controlled in order to vary the output of the laser and to optimize the interaction between laser and the materials surface. The term E is the peak laser power within a single pulse, in kilowatts. This can be set in the range of 0 to 7 kW. The 2 to 7 kW peak powers were used in the experiments. The term L is the pulse width expressed in milliseconds. It can have values from 0.3 to 20 ms. The 10 and 8 ms pulse widths were used for the experiments reported here. The term R is the number of pulses per second, *i.e.*, frequency in Hertz. A value of 5.7 Hz was selected in these tests, although it is capable of varying from 0.1 to 1000 Hz. The total input energy in each laser pulse can be calculated using Eq 1.

$$\text{Energy} = E \cdot L \text{ Joules} \qquad \text{(Eq 1)}$$

The average power of the laser can be calculated using Eq 2.

$$\text{Average power} = E \cdot L \cdot R \text{ Watts} \qquad \text{(Eq 2)}$$

The maximum energy per pulse and the maximum average power that can be reached on the laser are 70 Joules and 400 Watts, respectively.

The morphologies of the surfaces and the cross sections of the laser-processed samples were examined using a Nikon EPIPHOT-TME optical microscope with Sony UP-5000 color video printer and Philips XL 30 scanning electron microscope (Philips Electronic Instruments Corp., Mahwah, NJ). The chemical compositions and oxidation states of the TiAl and Ti_3Al samples were analyzed using a Kratos (Manchester, UK) AXIS

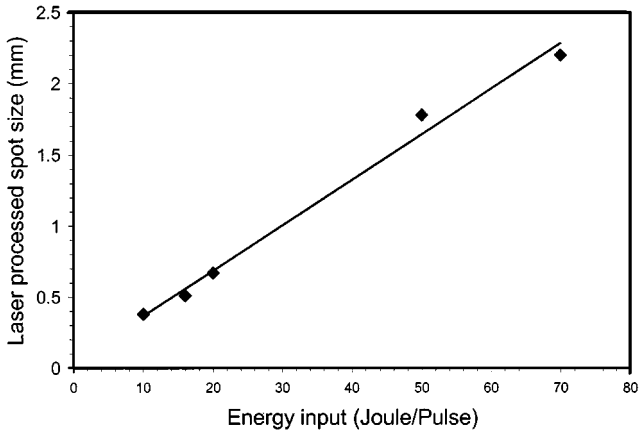

Fig. 2 Laser-processed spot size of TiAl intermetallic samples as a function of laser energy input per pulse (R = 5.7 Hz; L = 10 ms)

165 x-ray photoelectron/auger scanning surface analysis system with a monochromatic Al K_α x-ray source at pass energy of 80 eV. All the XPS spectra were referenced to contingent C 1s peak at 284.8 eV. An Ar ion gun was employed to do sputtering during depth profiling of the samples.

3. Results and Discussion

3.1 Al Content and Cracking

The key variables that affect a material's laser interaction, in laser surface processing, are laser power, beam size, scanning speed, and absorption of the laser beam to the material's surface. As a matter of fact, the key factors that control a material's laser interaction are the energy absorbed by the material's surface and the interaction time of the laser and the material. Since the Nd:YAG laser operates in pulse mode, most of the experiments were conducted under the conditions of single pulse, fixed frequency (R), and fixed length of pulse (L) and using focused beam. The only changing parameter was peak power (E), which changes the total energy input into the material's surface. At a fixed beam size, various energy inputs would cause different processed spot sizes, if considering effects of heat flow and diffusion processes. Depending on the absorbability and thermophysical properties of the material, the laser-processed spot sizes can be either larger or smaller than the beam size of the laser. Figure 2 shows the dependency of laser-processed spot sizes on the energy of laser for TiAl samples. The spots have circular shapes and the diameters of them are given in Fig. 2 as measurements of sizes. The boundaries are defined as the lines that distinguish the central processed areas and the unprocessed base metals by obvious morphological and color features. Along with an increase of the energy, the processed spot sizes increase linearly. The relationship between laser spot size and energy input is very important and it can be used as the base line for future reference, in the selection of appropriate processing parameters. It is also needed for the thermodynamic calculation of heat transfer and energy dissipation. Figure 3 shows an optical microscopic picture of laser-processed spots on TiAl. The centered white colored part is the laser-processed area. The

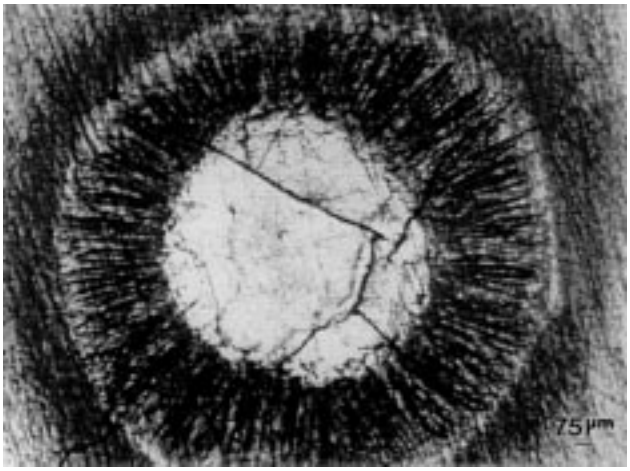

Fig. 3 Optical micrograph of a laser-processed spot on TiAl intermetallic; *E*, 2 kW; *L*, 10 ms; *R*, 5.7 Hz; 1 pulse

periphery blue color ring is the pileup of materials molten in the center and expelled out. In the laser processing process, the energy input into the material's surface may melt the surface layer of materials and vaporize a very small amount of material on the very thin surface layer. During removal of the surface atoms, a momentum impulse takes place and generates a shock wave. Although it is not like laser shock hardening processes, in which the shock wave can cause tremendous mechanical effect, which causes the presence of compressive stresses at the surface, the shock wave created here is strong enough to exclude the molten materials from the central molten pool to the periphery. The radical lines on the blue ring of Fig. 3 verify that the movement of those materials from the center out to the periphery took place during laser processing. Another obvious feature noticed on the optical micrograph is that several big cracks connected together inside the laser-processed spot and then spread out.

Figure 4(a) and (b) depict the SEM pictures of the laser-treated surfaces after polishing and etching. They clearly show that cracks developed inside the laser-processed spot and branched out along the grain boundaries. A magnified view (Fig. 4b) of the cracks shows that materials in the grain boundaries are broken into small pieces. When higher energy was input into the surface, more cracks developed, and they formed a net structure, as can be seen in Fig. 5. An SEM picture of the non-laser-processed area of TiAl is shown in Fig. 6, which illustrates that the TiAl sample has a fully transformed structure[17] with large grain sizes that are typically greater than 500 μm in diameter. All the grains contain γ/α_2 lamellae. Since the γ and α_2 laths in the lamellar structure have different orientations in different grains, as shown in Fig. 6, large strains would develop along different directions inside those grains during heating by the laser beam. The conflicts in strain between grains would cause plastic deformation. The grain boundaries that contain many defects, impurities, and intrinsic microcracks formed in the previous preparation process are likely to be cracked nucleation sites. The rapid heating and cooling in the laser treatment process would lead to the propagation and coalition of cracks along the grain boundaries.

When energy input into the surface was reduced, the surface

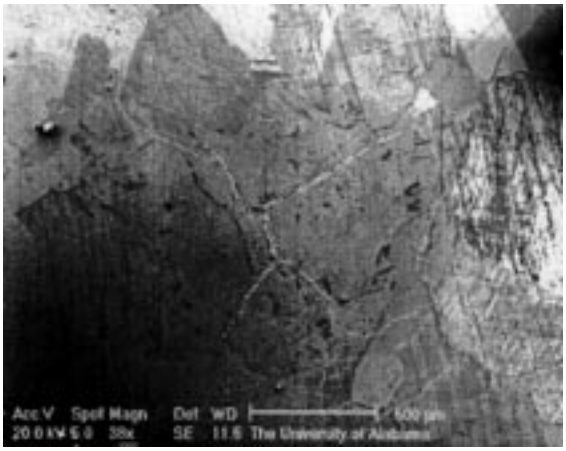

(**a**)

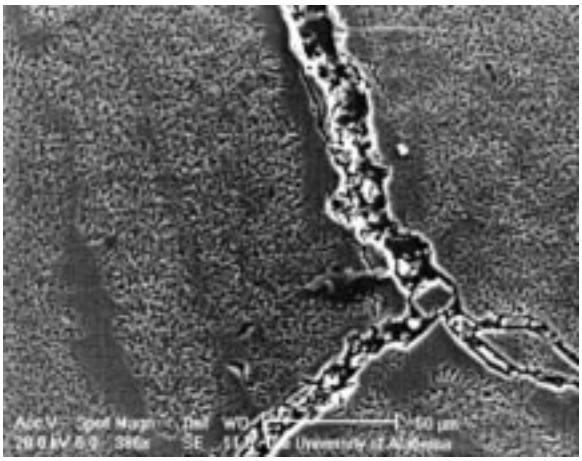

(**b**)

Fig. 4 (**a**) SEM photograph of a laser-processed surface on TiAl intermetallic after polishing and etching; *E*, 2 kW; *L*, 10 ms; *R*, 5.7 Hz; 1 pulse. (**b**) Local magnified view of (a)

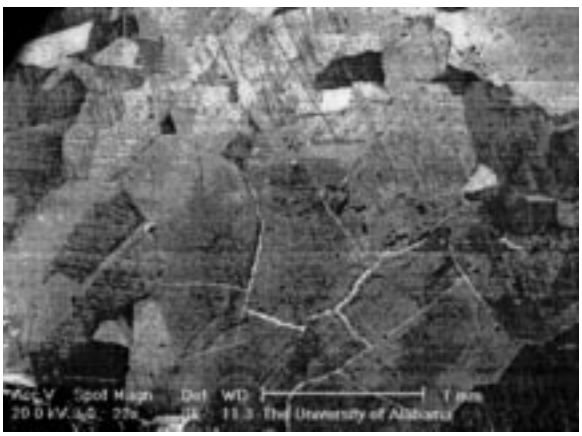

Fig. 5 SEM photograph of a laser-processed surface on TiAl intermetallic after polishing and etching; *E*, 7 kW; *L*, 10 ms; *R*, 5.7 Hz; 1 pulse

of TiAl might not have melted, as shown in Fig. 7. However, there are still big cracks in the laser-treated spot and they even

Fig. 6 SEM photograph of an unprocessed surface area on TiAl intermetallic after polishing and etching

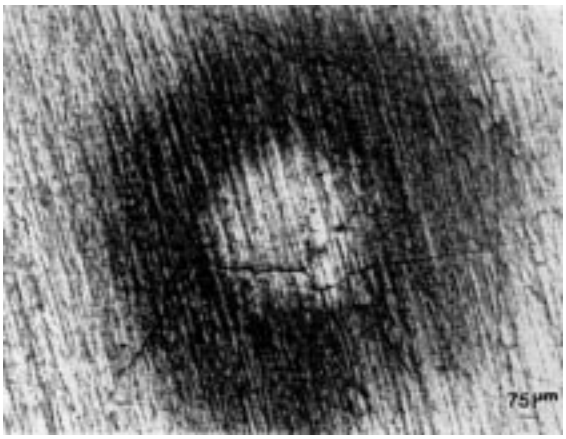

(**a**)

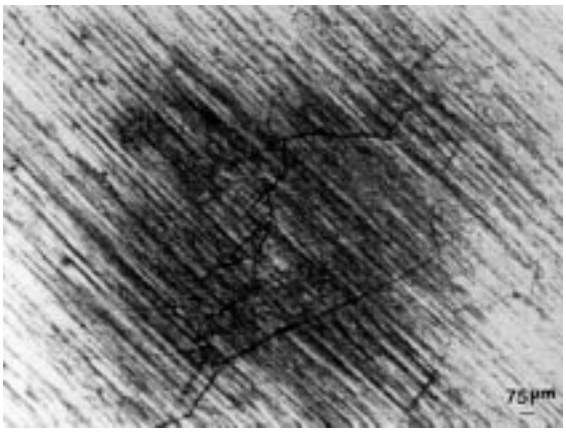

(**b**)

Fig. 7 Optical micrographs of a laser-processed spot on TiAl intermetallic; *L*, 8 ms; *R*, 5.7 Hz: (**a**) *E*, 2 kW and 1 pulse; and (**b**) *E*, 1 kW and 3 pulse

stretched out to the unprocessed areas. This indicates that the cracks in the laser-processed TiAl samples can initiate and develop without surface melting and the resolidification process. The rapid expansion and contraction caused by fast heating and cooling are strong enough to result in separation between grains. It seems clear that the resolidification process does not contribute too much to the crack formation. This is why no appreciable difference can be seen on the appearance of cracks of laser melting spots (Fig. 5) and no-melting spots (Fig. 7), except that there are more cracks in the former than in the latter. The optical microscopy of a multipulse laser-processed spot is shown in Fig. 8. It is reasoned that the first laser pulse brings in the long and large cracks along the grain boundaries and successive laser pulses cause the cracks to branch across the grains.

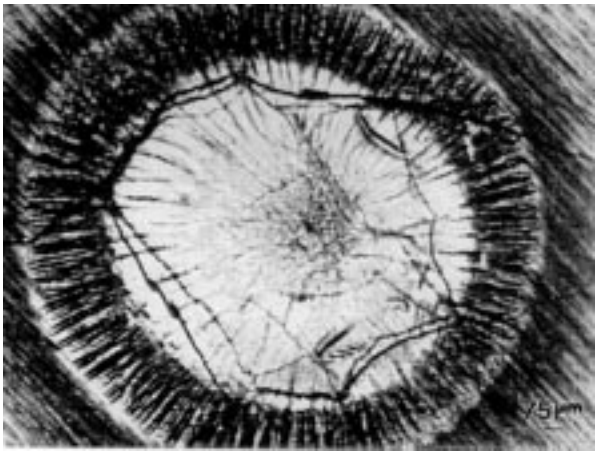

Fig. 8 (**a**) to (**d**) Optical micrographs of a laser-processed spot on TiAl intermetallic; *E*, 2 kw; *L*, 8 ms; *R*, 5.7 Hz; 3 pulse

Figure 9 presents optical micrographs of the spots of pure Ti, Ti_3Al, TiAl, $TiAl_3$, and 2024 Al alloys processed by laser beam under the same conditions. No cracks can be found on the surface of pure Ti sample after laser melting. This means pure Ti has an excellent ductility and a good thermal shock resistance. A few small cracks on the Ti_3Al sample surface were observed under the microscope, but they are difficult to see in the picture under current magnification. As the Al content in the Ti-Al alloy approaches 50, there are several large cracks that develop after laser treatment. Further, more cracks can be seen inside the laser-processed spot on $TiAl_3$. In the 2024 Al alloy, the Al element is the predominant composition, not only did many large cracks develop inside the laser-processed spot, but these cracks propagated far into the nonprocessed area. Therefore, it is obvious that the greater the Al content in the Ti-Al alloys, the greater the number of and the larger the cracks that will develop in the laser-processed area of those alloys. It is thought that the reason for this is that the Al content in the Ti-Al alloy has important effects on the properties of the grain boundary.

3.2 Surface Enrichment of Al Element and Oxidation

The direct interaction between the laser beam and the material being processed can cause dramatic changes in the microstructure and composition of the material's surface. Temperature and cooling rate could be the most important factors among all factors in dominating the final results of a laser/material interaction. However, direct measurement is not an easy

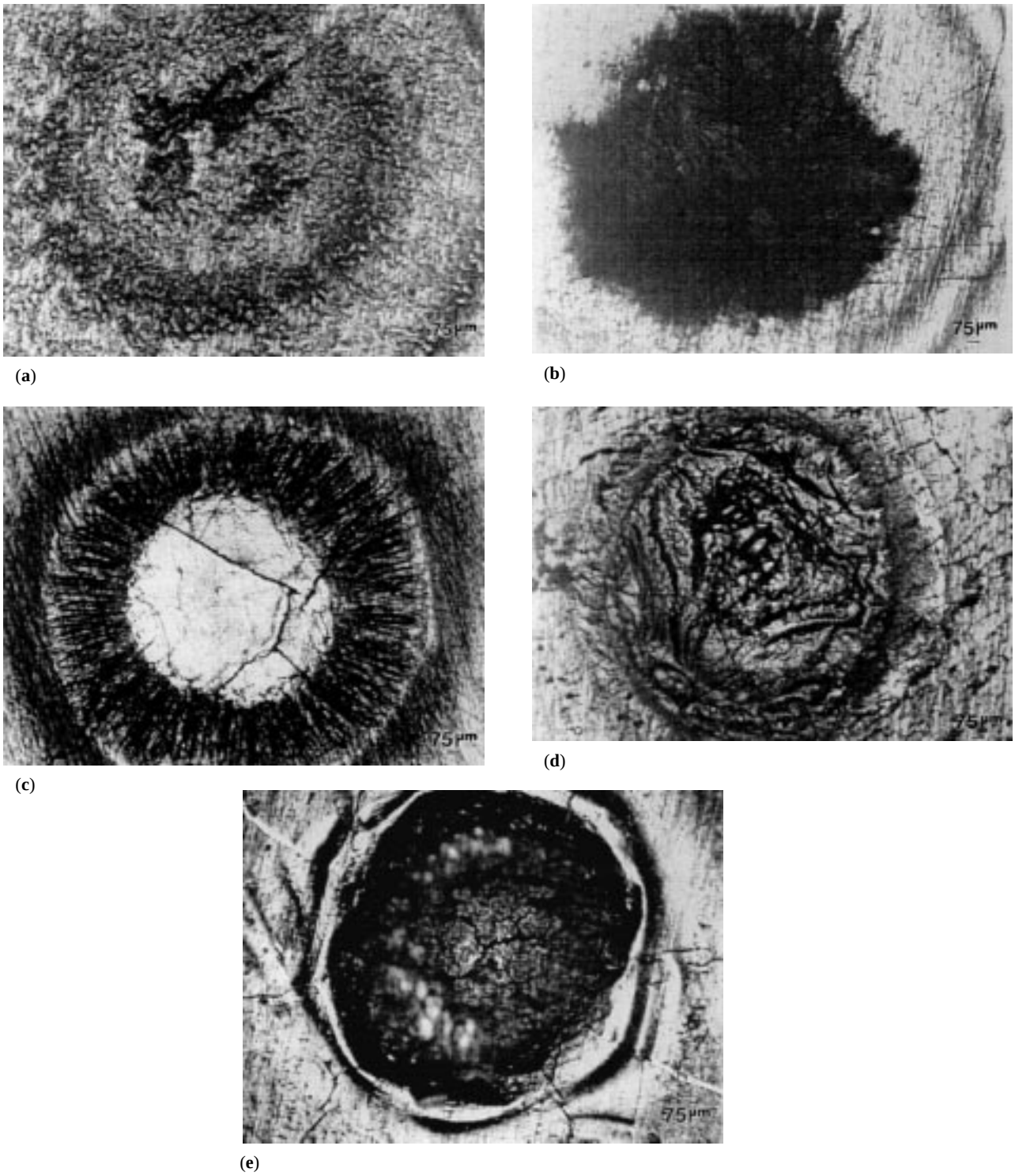

(**a**) (**b**) (**c**) (**d**) (**e**)

Fig. 9 Optical micrographs of laser-processed spots on (**a**) pure Ti, (**b**) Ti_3Al, (**c**) TiAl, (**d**) $TiAl_3$, and (**e**) 2024 Al alloy; *E*, 2 kW; *L*, 10 ms; *R*, 5.7 Hz; 1 pulse

approach to measure them. As shown in Fig. 10, for laser-processed TiAl intermetallic, surface colors inside the laser-processed spots are very rich for varying treatment parameters, or even for one spot. For the sample processed under an energy of 70 J/pulse, the surface colors from the center to the periphery pile-up of the materials are dark blue, pink, yellow, white, and blue. When considering a rectangular shape energy pulse shining on the surface of the samples, the temperature would have great gradients along the radii of the laser spot because of fast heat flow or heat transfer into base metal. Thus, the

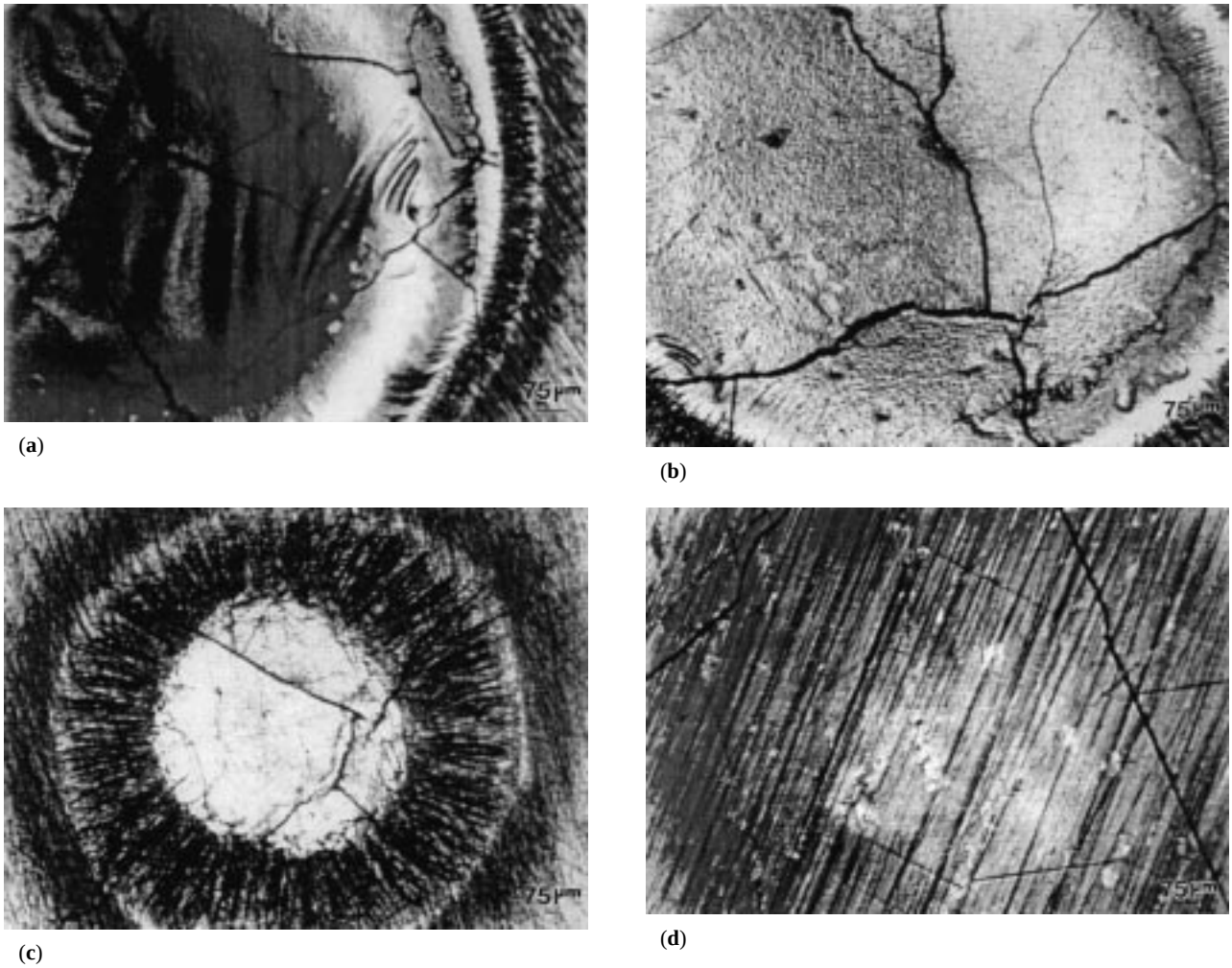

(**a**) (**b**) (**c**) (**d**)

Fig. 10 Optical micrographs of laser-processed spots on TiAl intermetallic samples; *L*, 10 ms; *R*, 5.7 Hz; 1 pulse: (**a**) *E*, 7 kW; (**b**) *E*, 5 kW; (**c**) *E*, 2 kW; and (**d**) *E*, 1 kW

center of the processed spot has the highest temperature and the outermost layer has the lowest temperature. It is interesting to note that when lower energies were used for the laser processing of TiAl samples, the colors in each individual spot looks alot like a part of spectrum of the ones processed with higher energies. For instance, the sample processed under energy of 50 J/pulse has yellow, white, and blue colors from the center of the spot out. The main color for the one processed under 20 J/pulse is white, while the one processed in 10 J/pulse has a blue color. Therefore, one could speculate that similar microstructural, chemical, and compositional changes might have occurred in the same color areas, although they were processed under different laser processing parameters. To confirm this point, more detailed and specially designed experiments are necessary.

The XPS experiments have been performed on the laser-processed and unprocessed TiAl intermetallics in order to partially clarify the above speculation as well as to study the surface chemical changes that could have been caused by laser surface processing. Figures 11 and 12 show XPS spectra of Al 2p and Ti 2p on the surfaces of the samples with or without Ar ion sputtering for 6 min. It is clear that before ion sputtering there is a natural oxide film on the unprocessed sample surface. Thus, Ti 2p 3/2 and Al 2p have binding energies of 459 and 74.5 eV, which correspond to the binding energies of Ti 2p 3/2 and Al 2p in TiO_2 and Al_2O_3 oxides, respectively. After elimination of the oxide film with sputtering, the binding energies for Ti 2p 3/2 and Al 2p are 454.3 and 72.7 eV. These values are very close to their values in pure metal forms, although they should be considered as the binding energies for them in intermetallic compounds. Figure 12 shows the results of XPS analysis for the laser-processed TiAl sample. The binding energies for Al 2p before and after sputtering are almost the same, around 74.6 eV, which indicates that Al_2O_3 oxide is the only form of Al element within the analyzed depth. However, as shown in Fig. 10(b), the existing form of the Ti on the laser-processed surface is TiO_2, as indicated by the binding energy of Ti 2p 3/2 at 459.4 eV. After sputtering of 6 min by Ar ions, the XPS spectrum of Ti 2p 3/2 shows two peaks: one main peak at 459.0 eV and a small shoulder peak at 455.5 eV. They are considered as the binding energies of Ti 2p 3/2 in TiO_2 and TiO, respectively. This means that inside the surface layer of the laser-processed sample, TiO exists as another form of Ti oxide.

Figure 13 illustrates the depth profiles of elements C, O, Ti,

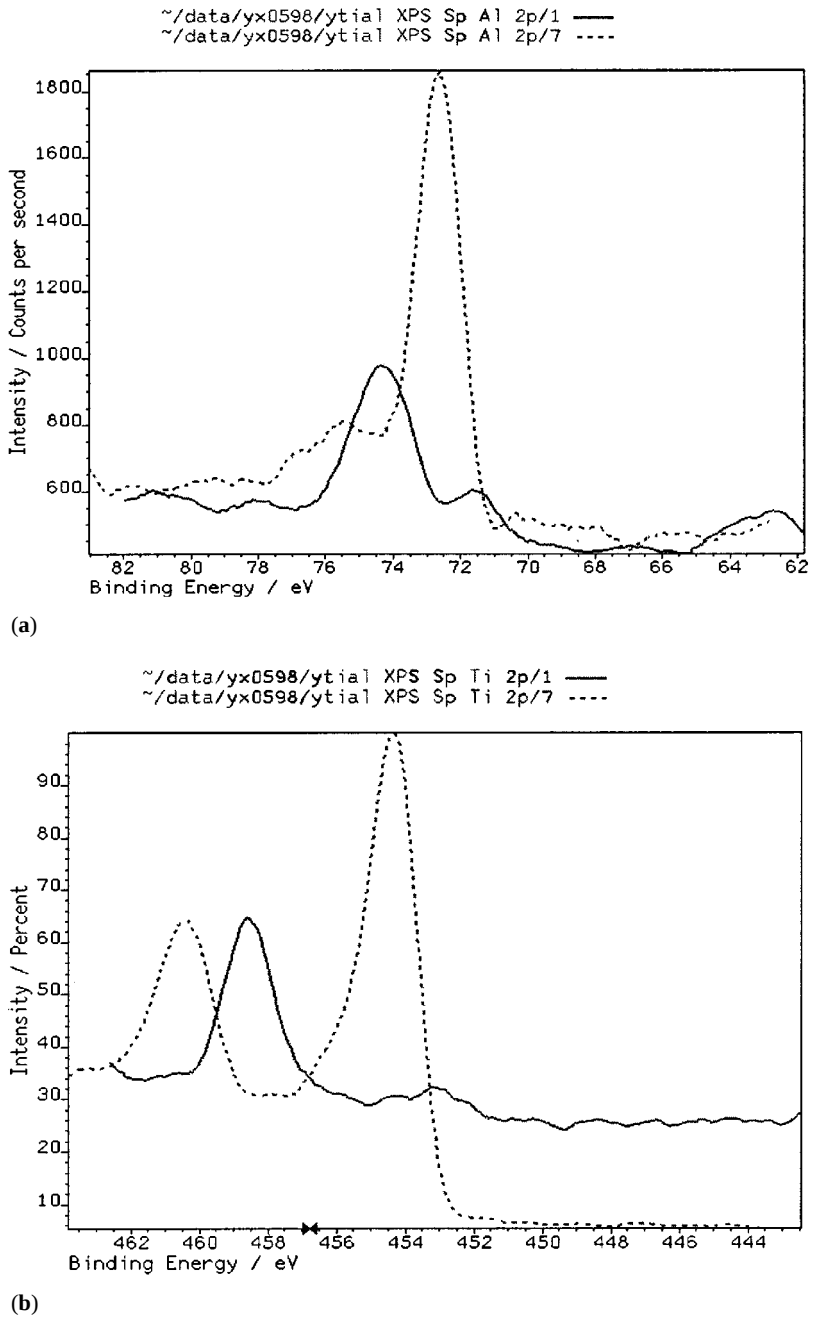

Fig. 11 XPS spectra of (**a**) Al 2p and (**b**) Ti 2p on the surface of unprocessed TiAl intermetallic before and after Ar ion sputtering

and Al in the laser-processed TiAl, Ti_3Al, and unprocessed TiAl samples. It can be seen from Fig. 12(a) that the C-containing adsorbates and the natural oxide film dominate the outermost surface of the unprocessed sample. In this region, Ti and Al contents are low, with more Al over Ti relatively. Along with the sputtering, C and O contents decrease while Ti and Al contents increase. After about a 5 min sputtering, Ti and Al become the main components and the contents of C and O become relatively low. It also can be noticed that at this region, the content of Ti is more than that of Al, although the difference is just about 5 at.%. When considering the XPS spectra in Fig. 10, it can be concluded that there is more Al than Ti in the natural oxide film. Laser processing of TiAl and Ti_3Al, resulted in an excessive oxidation of the surfaces, as shown by XPS spectra in Fig. 11. The chemical composition distributions along the depth (sputtering time) are nearly uniform in the sputtered time scales, except those deviations caused by C-containing adsorbates in the outermost shallow layers. Oxygen is a prominent element on the surfaces, which has a 75 at.% concentration. The total content of Al and Ti elements is only about 25 at.%. The complete oxidation of Al and Ti as Al_2O_3, TiO_2, and TiO would not consume all the oxygen content shown in the depth profile; it is thought that the surplus oxygen is absorbed as O_2 gas on the sample during laser processing. As observed, the

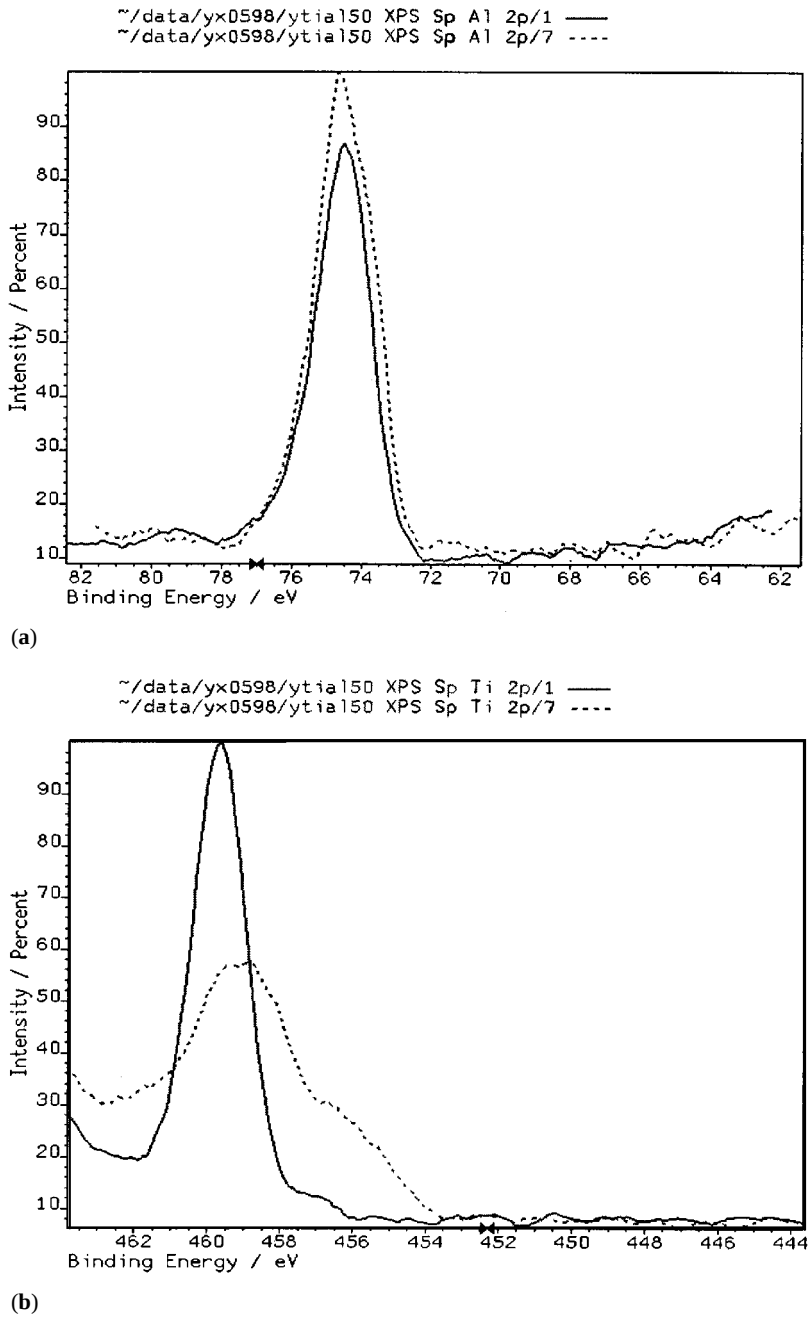

Fig. 12 XPS spectra of (**a**) Al 2p and (**b**) Ti 2p on the surface of laser-processed TiAl intermetallic before and after Ar ion sputtering; *E*, 5 kW; *L*, 10 ms; *R*, 5.7 Hz, 1 pulse

laser-processed surfaces have porous structures. Oxygen can be absorbed to the surfaces and some could be trapped in the pores during laser processing. Another important result from these depth profiles is that the Al-to-Ti ratio in the oxidation layers on the laser-processed sample surfaces is larger than that in the unprocessed bulk intermetallic compounds. For example, in the Ti_3Al sample, the Ti-to-Al ratio should be around 3 to 1, but inside the oxidation layer, the ratio is nearly 1 to 1. In the TiAl bulk materials, the Ti-to-Al ratio is almost 1, while in the oxidation layers, more Al is determined. The enrichment of Al in the oxidation layers of laser-processed Ti-Al intermetallic compounds can be caused by the larger solid diffusion rate of Al over Ti and/or flow segregation in the molten pool resulting from wetability and surface tension during laser processing. At lower laser input energy, the enrichment of Al in the oxidation layer can also be seen. As the input energy increases, the phenomenon becomes more obvious. The content of Al can be 2 times more than that of Ti in the layer, as can be seen from Fig. 13(c). Further, an increase of the energy input does not greatly affect the ratio between Al and Ti.

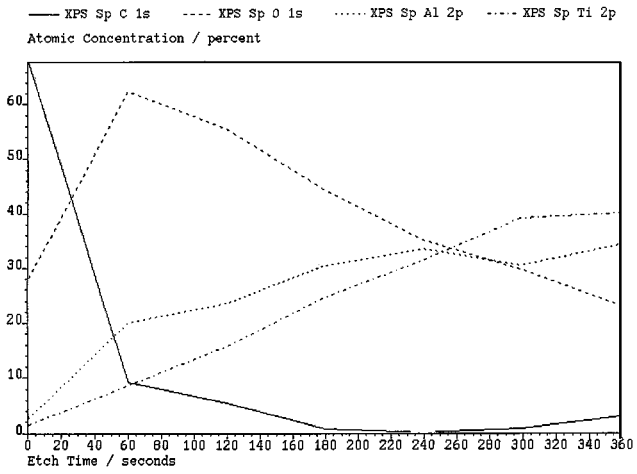

(**a**)

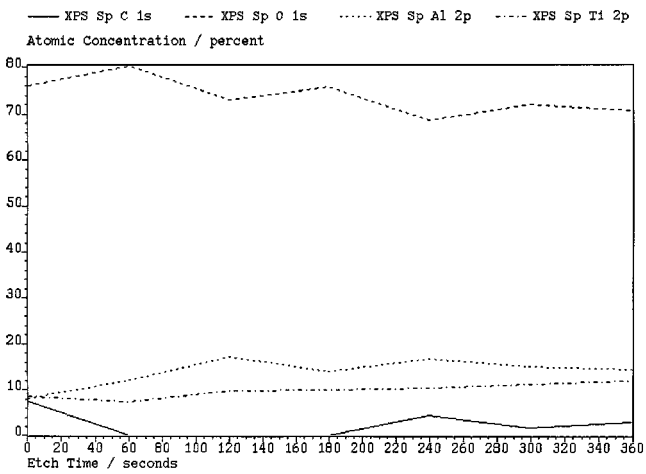

(**b**)

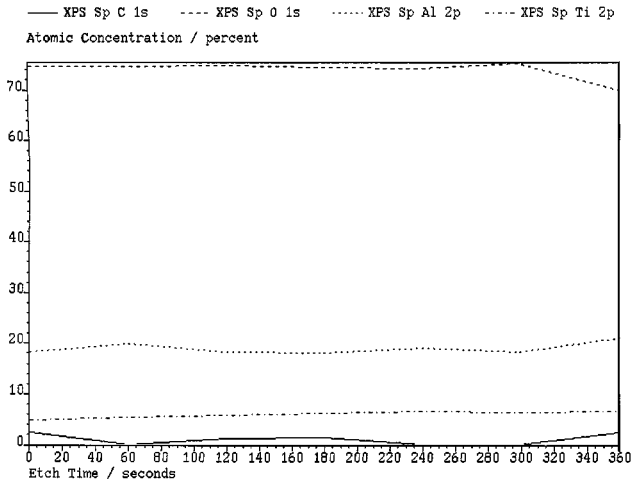

(**c**)

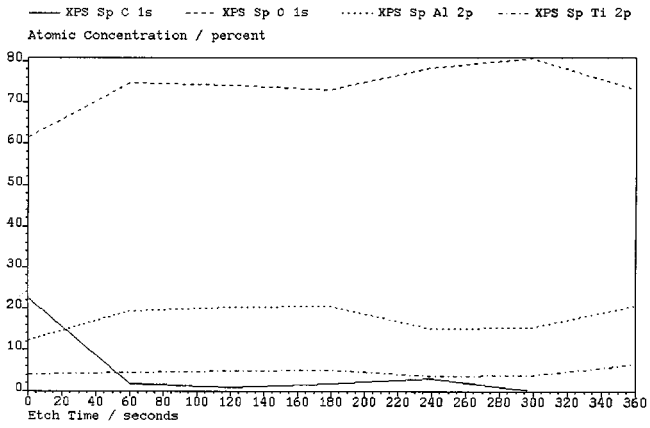

(**d**)

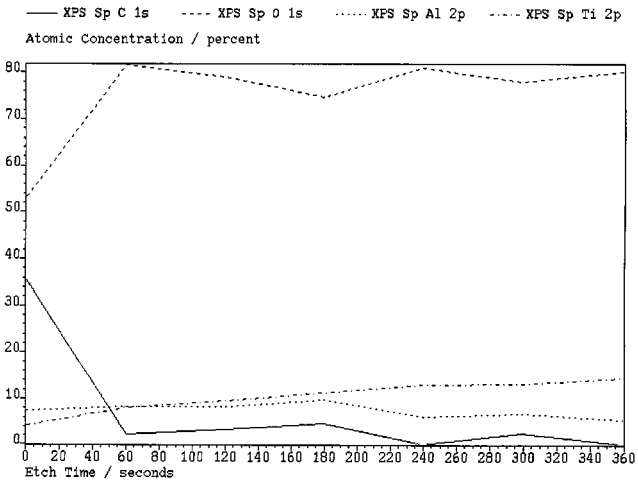

(**e**)

Fig. 13 Sputtering depth profiles of elements C, O, Ti, and Al on the surfaces of (**a**) unprocessed TiAl intermetallic, laser-processed TiAl intermetallic at power *E* values of (**b**) 1 kW, (**c**) 2 kW, (**d**) 7 kW, and (**e**) laser-processed Ti_3Al intermetallic at power of 2 kW

Although the mechanisms that control the enrichment of Al in the oxidation layer of laser-processed Ti-Al intermetallics are not clear at this stage, the results differ from the high-temperature oxidation results observed for TiAl alloys, where Ti-rich scales in the outermost layer were observed.[15,16,18,19] It is possible that rapid heating and quenching during laser processing would vary diffusion rates, the growth rate of oxides, *etc.*, which could affect the distributions of Ti and Al in the oxide scales. At the same time, surface melting and fluid flow in the laser processing of Ti-Al intermetallics are the processes that do not happen in the oxidation processes, but they can vary the distributions of the elements in the oxidation layers of laser-processed samples. Oxidation studies of Ti-Al intermetallics are complicated, so further experiments need to be carried out from this point.

4. Conclusions

A series of Ti-Al alloys including pure Ti, Ti-Al intermetallic compounds, and 2024 Al alloy have been processed by using a Nd-YAG laser. Cracks along grain boundaries caused by rapid heating and cooling of laser processing are the dominant characteristics of surface morphology of laser-processed samples. As the Al content in the samples increases, so does the amount and size of the cracks found on the samples after laser processing under the same conditions. A linear relationship between the laser-processed spot size and the energy inputs was found and plotted out. The surface oxidation layers of the laser-processed samples are studied using XPS with Ar ion sputtering. The oxidation layers consist of Al_2O_3, TiO_2, TiO, and adsorbed O_2. The Al enrichment is found in natural oxide film of TiAl as well as the oxidation layer formed on the surfaces of TiAl and Ti_3Al intermetallics processed by pulsed laser, which is different from the results observed for traditional oxidation of TiAl at elevated temperature.

Acknowledgments

This research was performed under appointment to the Advanced Industrial Material Program, which is administered by Oak Ridge Institute for Science and Education for the United States Department of Energy and Oak Ridge National Laboratory. We also thank the Department of Metallurgical and Materials Engineering, The University of Alabama, for additional funding. This work was also supported by the National Science Foundation.

References

1. M. Yamaguchi: in *Titanium '92-Science and Technology*, F.H. Froes and I. Caplan, eds., TMS, Warrendale, PA, 1993, p. 959.
2. W. Thompson and W. Chu: in *Microstructure/Property Relationships in Titanium Aluminides and Alloys*, Y.-W. Kim and R.R. Boyer, eds., TMS, Warrendale, PA, 1991, p. 165.
3. P.S. Liu, K.H. Hou, W.A. Baeslack III, and J. Hurley: in *Titanium '92-Science and Technology*, F.H. Froes and I. Caplan, eds., TMS, Warrendale, PA, 1993, p. 1477.
4. S.G. Kumar, R.G. Reddy, and L. Brewer: *J. Phase Equilibria*, 1994, vol. 15 (3), pp. 279-84.
5. S.G. Kumar, R.G. Reddy, J. Wu, and J. Holthus: *J. Mater. Eng. Performance*, 1995, vol. 4, pp. 63-69.
6. S.G. Kumar and R.G. Reddy: *Proc. Int. Symp. on Synthesis/Processing of Lightweight Metallic Materials*, TMS, Warrendale, PA, 1995, pp. 129-39.
7. S.G. Kumar and R.G. Reddy: *Metall. Mater. Trans. A*, 1996, vol. 27A, pp. 1121-26.
8. J. Mazumder: in *Laser Materials Processing*, M. Bass, ed., North-Holland Publishing Company, Amsterdam, Netherlands, 1983, p. 112.
9. W.M. Steen and J.N. Kamalu in *Laser Materials Processing*, M. Bass, ed., North-Holland Publishing Company, Amsterdam, Netherlands, 1983, p. 15.
10. M Querry: in *High Power Lasers*, A. Niku-Lari and B.L. Mordike, eds., Pergamon Press, Elmsford, NY, 1989, p. 195.
11. J.C. Beitialarrangoitia, G.E. Garcia de Vicuna, and S.K. Ghosh: in *High Power Lasers*, A. Niku-Lari and B.L. Mordike, eds., Pergamon Press, Elmsford, NY, 1989, p. 213.
12. M.J. Hsu and P.A. Molian: *J. Mater. Sci.*, 1994, vol. 29, p. 5607.
13. K. Li and P. Sheng: in *Manufacturing Science and Engineering-1995*, E. Kannatey-Asibu, Jr., C.J. Li, Y. Rong, C.-Y. Shia, and F.J. Stango, eds., ASME, New York, NY, 1995, vol. 1, p.3.
14. S. Tsukamoto and O. Umezawa: *Mater. Sci. Eng.*, 1997, vol. A223, p. 99.
15. X. Wen and R.G. Reddy: *Processing and Fabrication of Advanced Materials V*, TMS, Warrendale, PA, 1996, pp. 37-389.
16. R.G. Reddy, X. Wen, and Y. Li: in *Titanium Extraction and Processing*, B. Mishra and G.J. Kipouros, eds., TMS, Warrendale, PA, 1997, pp. 153-61.
17. S. Huang and D.S. Shih: in *Microstructure/Property Relationships in Titanium Aluminides and Alloys*, Y.-W. Kim and R.R. Boyer, eds., TMS, Warrendale, PA, 1991, p. 105.
18. J.U. Ejiofer, G.F. Fernando, and R.G. Reddy: *J. Mater. Sci.*, 1998, vol. 33, pp. 4029-33.
19. C.I. Okafor and R.G. Reddy: *JOM*, 1999, vol. 47, pp. 35-39.